J. Res. Inst. Catalysis, Hokkaido Univ., Vol. 31, Nos. 2/3, pp. 77 to 94 (1983)

OPTIMIZATION OF AN ANODIC ELECTROCATALYST: RuO_2/TiO_2 ON TITANIUM

By

M. D. SPASOJEVIĆ*), N. V. KRSTAJIĆ*)
and M. M. JAKŠIĆ**)

(Received July 13, 1983; in revised form October 11, 1983)

Abstract

An anodic electrocatalyst has been optimized as follows: It has a titanium substrate with a catalyst of RuO_2/TiO_2 and is designed for use in caustic-chlorine cells, chlorate cells, sea water electrolysis and similar applications. Its performance was rated by measuring the anodic potential at constant current versus time, by Tafel curves and by the durability (time to failure). Charging currents, electrode charge and crystal structure were also investigated and interrelated with the catalyst activity. The processing variables used to alter the properties were the mole fraction of RuO_2 in the coating, thermal treatment (temperature and time) and the catalyst loading. It has been pointed out that there exists an interrelating optimum for the mixed RuO_2/TiO_2 rutile phase structure, its composition (mole fraction) and the total amount (catalyst loading) as a function of thermal processing conditions (both time dependence and temperature) with steady-state polarization characteristics (electrocatalytic activity), corrosion stability and the life-time, which mutually coincide and make the basis for the optimization of catalytic coating.

Introduction

Catalytically activated titanium anodes and semi-permeable cationic membranes for chlorine cells are among the most important recent achievements in electrochemistry (1～4). For this reason, much work has been done on titanium electrodes during the last fifteen years, enriching the field with many reliable papers (5～75). The present study describes the optimization of an electrocatalyst for titanium anodes intended for use in chlorine and chlorate cells, sea-water electrolysis, etc.

The main criteria for electrocatalytic activity is the electrode overpotential as a function of current density, duration of electrolysis and the amount of

*) Institute for Electrochemistry—ICHTM, Belgrade, Yugoslavia.
**) Institute of Food Technology and Biochemistry, Yugoslavia Faculty of Agriculture, University of Belgrade, Belgrade, Yugoslavia.

noble metal. The best coating gives the smallest overpotential, the greatest lifetime at this overpotential and the minimum usage of precious metal, under industrial current density conditions. Several processing and structural features of the coating have been investigated in order to correlate them with the activity and durability. These are:

(a) The effect of the molar % of RuO_2 in the RuO_2/TiO_2 mixture on the crystal structure, surface state and catalytic activity as a function of time.
(b) The effect of the catalyst's temperature and baking time during thermal processing on its corrosion stability and catalytic activity, both being measured over a period of time.
(c) The effect of the catalyst loading on the catalyst's crystal structure, activity and durability. This effect was measured at the optimum RuO_2 mole %.

Correlating the activity and durability measurements with the processing variables and structural properties led to a composition, loading and heat treatment which gave the optimal catalytic activity and durability.

Experimental

To obtain reproducible data and draw reliable conclusions, special care was taken to process the electrodes under strictly identical conditions. The smooth titanium substrate was first roughened to increase its surface area and provide better coating adhesion. Best results were obtained by shotblasting with small steel balls (0.1 to 1.0 mm dia.). This gave good surface development with smooth rounded edges whereas sandblasting gave sharp edges (where the coating corrodes faster) and deeply embedded particles which were not completely removed by subsequent pickling.

The roughened samples were thoroughly degreased in ethanol saturated with sodium hydroxide at room temperature. After rinsing with distilled water, they were pickled for about 20 minutes in boiling 20% HCl. To remove other impurities, the samples were briefly immersed in warm 10% HNO_3, rinsed thoroughly in distilled water and dried in hot air.

As a solvent for the catalyst, water, butanol, anisole and isopropanol among others were tested. Isopropanol was chosen because its low surface tension gave uniform catalyst distribution while its high vapour pressure allowed rapid drying (25). $RuCl_3 \cdot 3H_2O$ (Johnson and Matthey) was first dissolved in 20% HCl, dried completely and then dissolved in isopropanol together with $TiCl_4$ (Merck) to produce a solution containing 10 g/L based on the pure metals (25). All chemicals were reagent grade purity. This solution was painted onto the titanium samples in successive layers until the desired

loading was attained. Each layer was dried at 50°C (which provided the best catalyst microdistribution) and then heated in air to 450°C for about 10 minutes. Drying at higher than 50° gave a porous film that was less mechanically stable. Usually five layers gave a metal loading of about 10 g/m². The loading was varied by applying fewer or more layers and the % RuO_2 was varied by making up solutions of different compositions but with the same total metal concentration. The final baking was carried out in an electric furnace at 500°C for 60 minutes. A Phillips PW 1730 diffractometer with a vertical goniometer PW 1050 and a static non-rotating sample carrier was used for X-ray diffraction analyses. This had a 35 kV, 20 mA power supply for copper excitation, and an AMR graphite monochromator. Phases were identified by reference to ASTM tables.

Steady state polarization and linear potential sweep measurements were carried out with the usual electrical set-up consisting of a potentiostat (Stonehard, model BC-1200), a PAR function programmer (Model 175), an XY recorder (Houston Instruments) and an oscilloscope (Tectronix, Model 564-B). The cell for both anodic polarization and cyclic voltammetry was a simple glass vessel (about 250 mℓ) with a double wall mantle for thermostatic temperature control (±0.2°C). The test electrodes were square plates with 1 cm² exposed geometric area on each side. They were mounted vertically and centred inside a Winkler platinum gauze cathode. Anode potentials were measured vs. a SCE by a VTVM (Keithly 610 C) but are reported vs the SHE. The tip of the Luggin capillary was about 0.3 mm in diameter and nearly touched the anode. Electrode potentials were corrected for ohmic losses by the interrupter technique and therefore represent true chlorine evolution potentials. The electrolyte was either concentrated (300 g/L) or dilute (30 g/L) sodium chloride in tripledistilled water. Lengthy polarization measurements to assess the durability of the catalysts were carried out in the same vessel at constant current, temperature, pH and electrolyte concentration.

Results and Discussion

1. *X-ray Diffraction Analyses of the Catalytic Coating*

X-ray diffraction analyses were carried out for all RuO_2 concentrations from 0 to 100%. Figure 1 is typical of a nearly optimal coating and shows peaks from the titanium substrate and from the rutile solid solution of RuO_2/TiO_2 whose d values are between those of the pure components (RuO_2 and TiO_2) (5, 29, 35, 37-40). Note the three peaks of the three rutile orientation planes (110) ($2\theta=27-28°$), (101) ($2\theta=35-36°$) and (211) ($2\theta=$

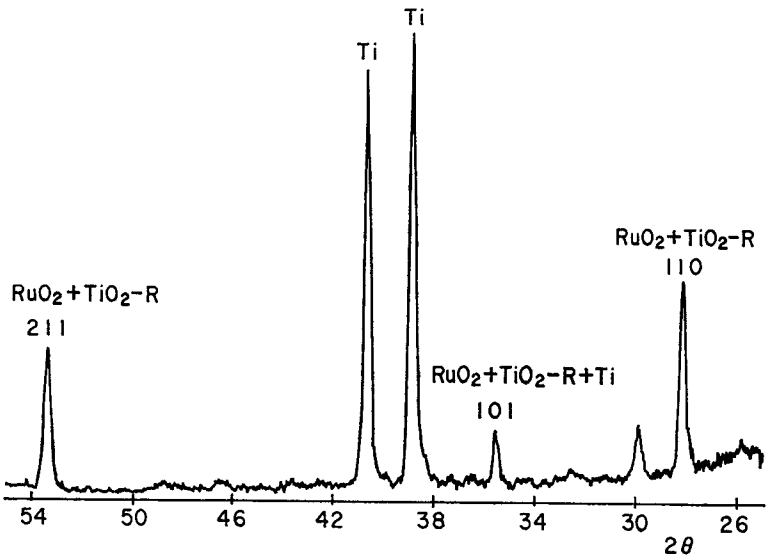

Fig. 1. X-ray diffraction radiograph for the composite electrocatalyst with optimal 40 mol. % in RuO_2 fraction.

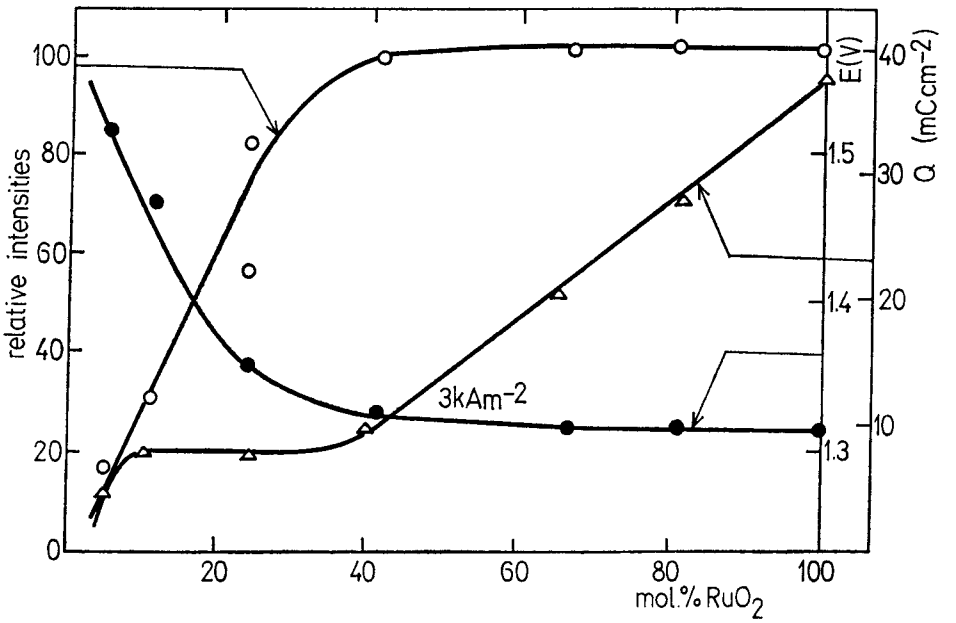

Fig. 2. The composite presentation of relative intensities for diffraction peaks of mixed rutile phase (the reflections for (110) rutile orientation plane), integral anodic charge and the anodic potential at constant current density (3 kA·m^{-2}) in function of molar RuO_2 fraction in $RuO/_2TiO_2$ catalytic coating.

53−54°). The absence of other peaks shows that all of the RuO_2 is present with TiO_2 as a solid solution with a rutile crystal structure. Diffraction peaks for anatase, which forms by thermal decomposition of pure $TiCl_4$ at 500°C, is found only in a coating with less than 5 mole % RuO_2. Some non-stoichiometric titanium oxides may form below 40% RuO_2 giving rise to indistinct peaks.

While X-ray diffraction has revealed the chemical composition of the coating, changes in the *d* values show a remarkable divergence from Vegard's law. Figure 2 shows how relative peak intensities due to rutile depend on the $\%RuO_2$. The fraction of rutile in the solid solution as shown by these peaks increases nearly linearly with $\%RuO_2$ until at about 40% only rutile is present in the coating. A dense homogeneous rutile structure is known to provide good electrocatalytic properties for chlorine evolution. (10)

2. *Electrocatalytic Activity vs $\%RuO_2$*

Electrocatalytic optimization of the coatings was carried out by obtaining polarization curves under the conditions used in industrial chlorine production (NaCl 300 g/L at 80°C and pH 2.0 to 2.5) (Fig. 3). Tafel lines at 40% RuO_2 or greater nearly coincide over a wide current density range (35). At 30 to 40% RuO_2 the plots from 0.01 to 1.0 kA/m^2 have two slopes, 30 mV/

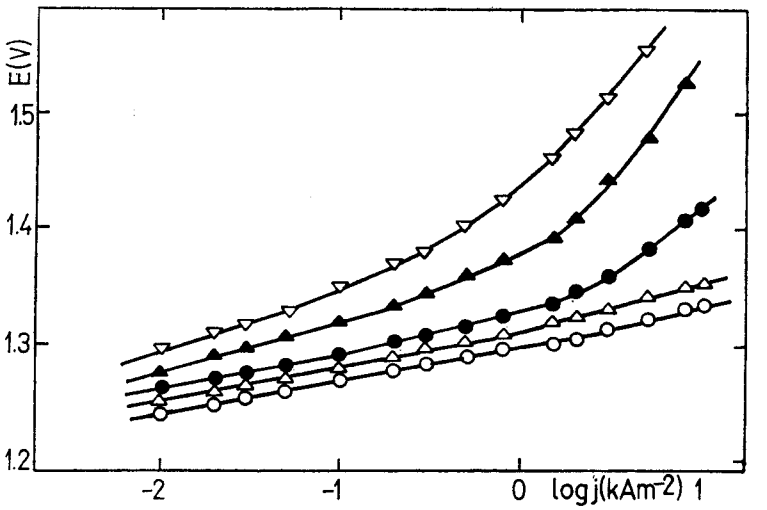

Fig. 3. Polarization characteristics for RuO_2/TiO_2 catalytic coatings of titanium anodes in brine (NaCl 300 $g \cdot dm^{-3}$, pH=2.0, 80°C) as a function of their composition for chlorine evolution reaction.

○—65–100 mol. % RuO_2, △—40 mol. % RuO_2, ●—25 mol. % RuO_2, ▲—10 mol. % RuO_2, ▽—5 mol. % RuO_2.

decade at lower current densities and 40 mV/decade at higher ones. This substantiates the mechanism proposed by Erenburg *et al.* (58, 59, 76, 77) The higher the RuO_2 content, the greater the current density range with the lower Tafel slope. At less than 30 mole % RuO_2, the Tafel slopes become progressively greater at low current densities and deviate from linearity at high current densities, the deviation being more pronounced and beginning at lower current densities as the % RuO_2 decreases.

Figure 2 shows the effect of % RuO_2 on the anode potential at 3 kA/m^2. It can be seen that the potential drops sharply as the % RuO_2 increases to about 40%, after which it asymptotically approaches its lowest value. This behaviour dramatically shows the scope for electrocatalytic optimization by changing the coating composition.

3. *Surface Properties of the Coating as a Function of %RuO_2*

It is well known that linear potential sweep voltammograms elucidate some surface properties of active coatings (18, 20, 26, 42). Figure 4 shows

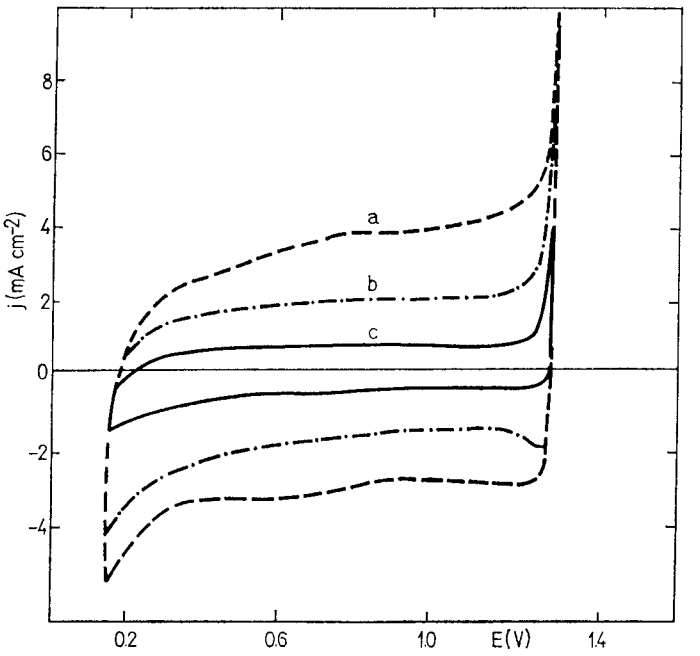

Fig. 4. Linear potential sweep voltammograms for various compositions of RuO_2/TiO_2 coating onto titanium anodes.

a—100 mol. % RuO_2, b—65 mol. % RuO_2, c—40 mol. % RuO_2 and the total amount of 10 $g \cdot m^{-2}$ in Ru+Ti (NaCl 300 $g \cdot dm^{-3}$, pH—2.0, 80°C). Potential sweep rate 50 mVs^{-1}.

how the voltammograms in brine change with the % RuO_2. Both the total area contained by the curves and the current peaks for Cl_2 and H_2 evolution increase with increasing RuO_2. The charging currents between the two gas-evolving reactions are unusually high. Above 40% RuO_2, the charging currents in the double layer region increase linearly with the RuO_2. The shape and potential of the current peaks, however, do not depend on the coating composition. This suggests that ruthenium atoms are the sole active centers for electrolysis and that their energy state and electroactivity are independent of the composition. TiO_2 is then an inert diluent in the rutile structure and does not affect the properties of the ruthenium atoms. This is the reason that the gas evolution potentials do not change with the % RuO_2 even though the current density increases.

The charging currents and the electrode charge in the double layer region between the two gas evolving reactions are of particular interest. Both of these reflect the state and activity of the coating and both change with the % RuO_2. The electrode charges were calculated by integration of the charging currents from the voltammograms in the region from 0.44 to 1.04 volts. Figure 2 shows how the charge depends on the % RuO_2 (42). There are three distinct charging regions, 0 to 10%, 10 to 40% and 40 to 100%.

At more than 40% RuO_2 the coating consists solely of rutile with varying concentrations of RuO_2. The linear increase of charging current with concentration is due to the increase in concentration and probably to an increase in porosity and hence of true surface area (43). Rutile coatings have the highest activity, giving a wider current density range with low Tafel slopes characteristic of barrierless chloride discharge as well as a wider total region of linear Tafel lines.

Figure 2 shows that the amount of rutile in the coating increases linearly with % RuO_2 in the 5 to 30% region (35, 39). The activity as shown by the electrode potential curve in Figure 2 has the same dependence. In addition, the electrical conductivity increases with RuO_2 as the nonstoichiometric TiO_2 and the non-homogeneous crystal structure decrease (5). The low conductivity at low RuO_2 concentrations causes the higher Tafel slopes and the deviations from linearity.

The presence of anatase TiO_2 at less than 5% RuO_2 also isolates the active centers and decreases the electrode charge. The intermediate region of constant electrode charge is probably due to a surface layer of rutile having a constant composition with nonstoichiometric titanium oxides underneath. Returning to Figure 2, it can be seen that the electrode reaches its optimal activity at 40 mole % RuO_2 and above.

4. *Durability as a Function of %RuO_2*

The change in the anode potential with time has been measured for chlorine evolution at 3 kA/m², 80°C and constant brine concentration to simulate industrial conditions. Figure 5 shows the anode potential versus time for various RuO_2 concentrations.

In all tests, the potential increased gradually at first, then more rapidly until at 1.4 V vs. S.H.E. there was a sudden electrode polarization accompanied by deterioration of the coating. These long term experiments show that durability is at a maximum at 40 mole % RuO_2 and decreases rapidly below 20%.

The extremely rapid corrosion below 20 mole % RuO_2 is probably due to further oxidation of the titanium substrate by anodically evolved oxygen. During thermal treatment, such coatings become enriched in titanium oxides with high electrical resistivity so that active RuO_2 centres are rather isolated. The TiO_2 acts as a site for further growth of the insulating layer which finally separates the catalyst from the substrate, causing the electrode to lose its activity (71, 72).

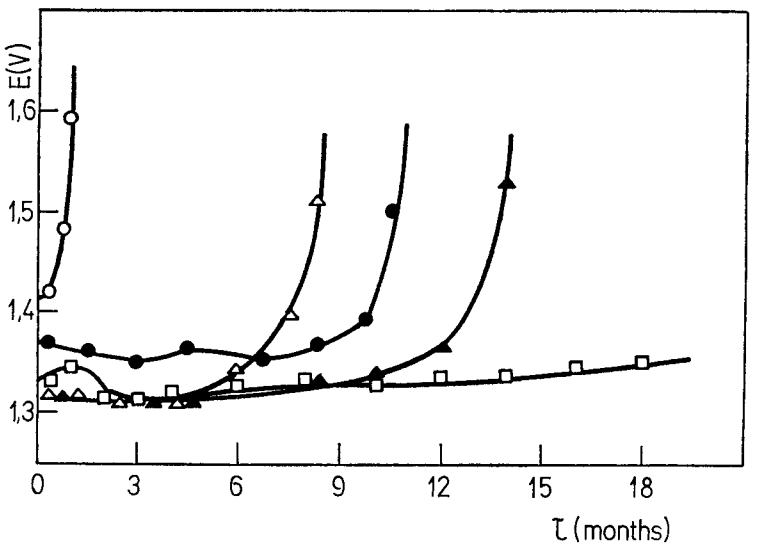

Fig. 5. The anode potential-time function at constant current density in brine electrolysis for various coating compositions.

○—10 mol. % RuO_2, ●—20 mol. % RuO_2, □—40 mol. % RuO_2, ▲—80 mol. % RuO_2, △—100 mol. % RuO_2 (3 kA·m^{-2}, NaCl 300 g·dm^{-3}, pH 2.0–2.5, 80°C).

At RuO_2 concentrations higher than the optimum, on the other hand, the rate of oxygen evolution increases (35, 79) so that the rate of oxidation of the substrate is increased. The more dense and homogeneous the coating, the slower the oxygen penetration and resulting electrode failure. The growth of an intermediate TiO_2 layer is consistent with the experimental fact that coatings enriched in RuO_2 down to the substrate show the greatest durability (69). It is noteworthy that at potentials more positive than 1.4 V vs. S.H.E., RuO_2 dissolves very rapidly resulting in immediate anode passivation (78).

Continuous tests simulating industrial conditions certainly afford reliable data on anode durability but require two or more years per test. For this reason, a shorter test was desirable and the following method has been employed concurrently with the previous one. The test anode was operated at a high current density (30 kA/m^2) at room temperature in dilute brine (30 g/L). These conditions give a potential greater than the critical value of 1.4 V where corrosion of the coating occurs within a few hours (Figure 5). In addition, high oxygen evolution in the dilute brine accelerates the rate of corrosion (70, 75). Figure 6 shows the duration of electrolysis before the

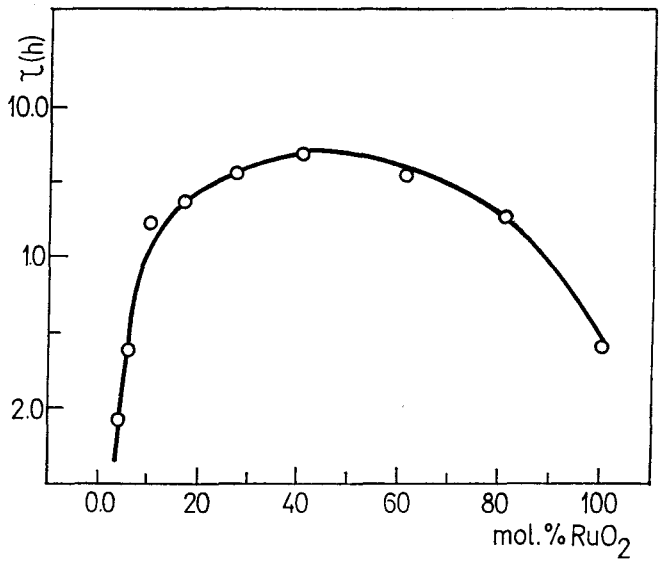

Fig. 6. The short stability test for the RuO_2/TiO_2 catalytic coating ploting the total stability time (τ(h)) as the duration before the sudden potential jump at 30 $kA \cdot m^{-2}$ in function of coating composition. (The electrolysis conditions : NaCl 30 $g \cdot dm^{-3}$, 25°C).

sudden increase in potential, plotted against the % RuO_2. This accelerated corrosion test, lasting less than 10 hours also gives a maximum durability between 30 and 60 mole %. Either method can be used as an indicator of corrosion stability and catalyst durability.

5. *Catalytic Activity as a Function of Baking Temperature*

The effect of temperature was determined by X-ray diffraction and by measurements of durability and catalytic activity. X-ray diffraction revealed that above 10% RuO_2, temperatures between 300 and 600°C give a homogeneous solid solution of rutile structure. Above 700°C, the peaks are split, corresponding to rutile RuO_2 and rutile TiO_2 (29, 40). With concentrations less than 10% RuO_2, temperatures between 300 and 600°C give anatase TiO_2 while above 700°C only rutile TiO_2 is found (29, 35, 38~40). Below 300° there is probably incomplete conversion of $TiCl_4$ to TiO_2 as shown by the small diffraction peaks for the mixed rutile structure in active coatings.

The mixed RuO_2/TiO_2 rutile coating thus has a limited temperature range in which it is stable (5). This conclusion is in agreement with the fact that no solid solution is formed when RuO_2 and TiO_2 are heated above 800°C for 100 hours or more, and that the mixed oxide formed at lower temperatures separates into its two components when heated strongly in an oxygen atmosphere. This change can be followed by observing the gradual shift of the diffraction peaks toward larger angles (15). Lower temperature treatment of the mixed crystal gives a decrease in peak width corresponding to a growth in crystal size. At 700°C average crystal lengths are 75 nm compared to 15 nm at 300°C.

The duration of thermal processing is another decisive variable for controlling the coating structure. An increase in time has an effect similar to that of an increase in temperature, *i. e.* increase in crystal size, increase in amount of conversion of chlorides to oxides below 300°C, increase in the separation of the mixed crystals into their components at high temperatures and an increase in oxidation of titanium. Titanium oxidation forms an insulating TiO_2 layer between the substrate and the active layer and eventually destroys the performance of the anode. It has been observed that an increase in oxygen concentration in the furnace also has an effect similar to an increase in temperature.

Catalytic activity and polarization properties depend on the coating structure and hence on the formation temperature and time (13, 14, 26, 29, 45, 57).

In Figure 7, anodic potentials are plotted against the logarithm of the current density for coatings with 40% RuO_2 which have been processed at various temperatures from 300 to 700°C. Between 400 and 500°C the

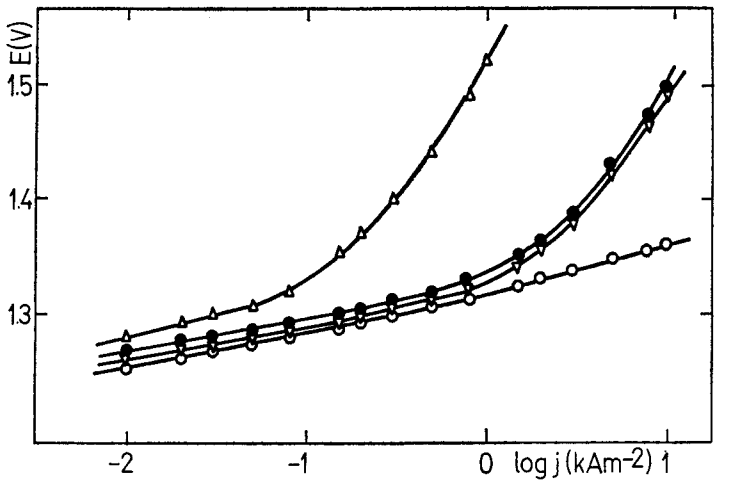

Fig. 7. Polarization characteristics of titanium anodes catalytically activated by 40 mol. % RuO_2 as a function of temperature for their thermal processing in chlorine evolution reaction.

●—300°C, ○—400-500°C, ▽—600°C, △—700°C (Electrolysis conditions NaCl 300g·dm^{-3}, pH 2, 80°C).

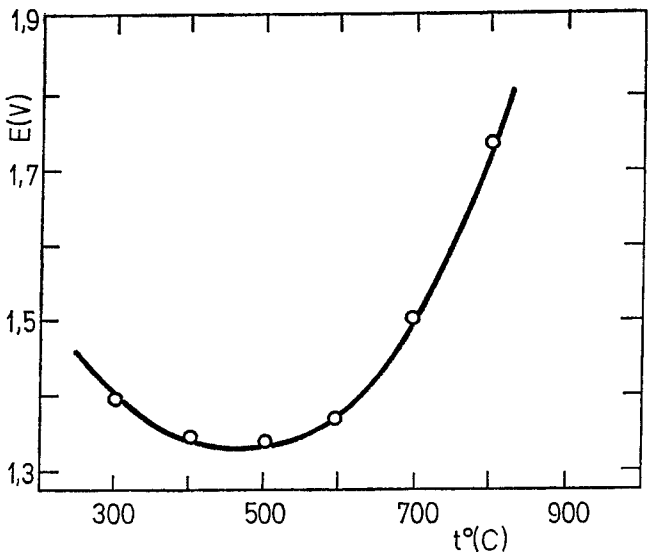

Fig. 8. The effect of temperature for thermal processing of titanium anodes on their potential at constant current density and for an optimal composition of catalyst (40 mol. % RuO_2). (Electrolysis conditions. NaCl 300 g·dm^{-3}, pH 2, 80°C, 3 kA·m^{-2}).

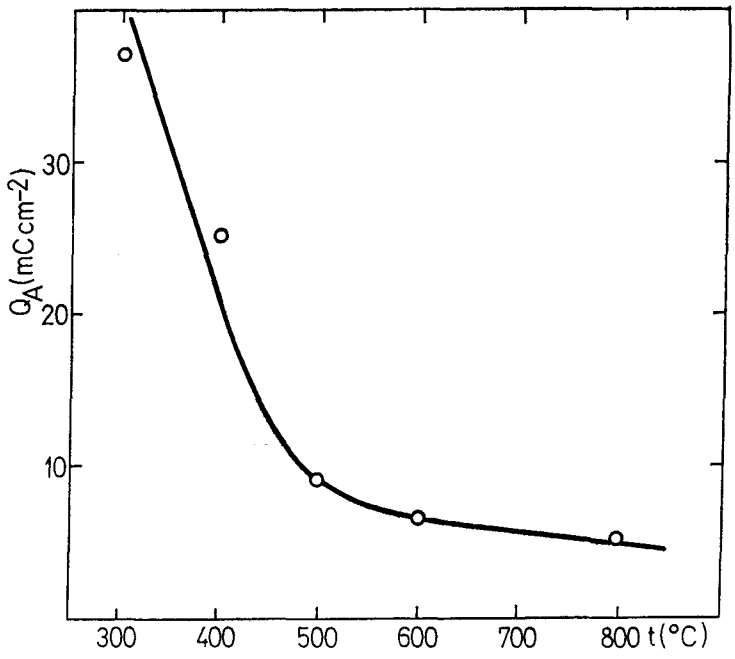

Fig. 9. The integral amount of anodic charge within the double layer region accounted from cyclic voltammograms in function of temperature for thermal processing of titanium electrodes (40 mol.% RuO_2).

coating potentials are low and follow a linear Tafel plot up to 10 kA/m^2. At higher and lower processing temperatures, the potentials are initially somewhat higher and rise above the Tafel slope at current densities that are lower as the temperature becomes further from the ideal. In Figure 8 the electrode potential at 3 kA/m^2 is plotted against formation temperature and this clearly shows the optimum temperature. At both lower and higher temperatures the activity decreases but above 600°C the catalyst durability decreases and the activity decreases more rapidly with time.

Cyclic voltammograms have the same shapes and potentials for all formation temperatures but the current peaks between the H_2 and Cl_2 evolution potentials decrease as the temperature increases. The anodic charge in the double layer region decreases rapidly with rising temperature until about 500°C when it becomes more nearly constant. This behaviour is caused by decreased surface area due to sintering and smoothing as well as by oxidation of titanium to insulating TiO_2 at higher temperatures.

Corrosion stability is greatest between 400 and 550°C with a gradual decrease at higher and lower temperatures. The accelerated corrosion test

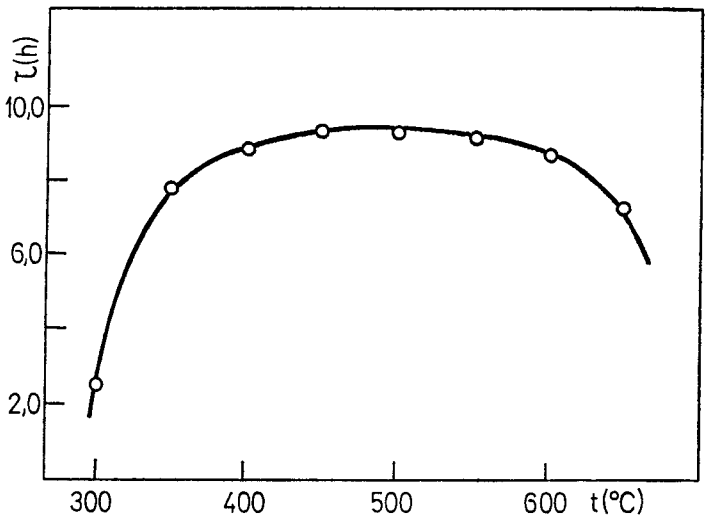

Fig. 10. The short stability test for the catalytic coating (40 mol. % RuO_2) ploting the total stability time (τ(h)) as the duration before the sudden potential jump at high current density in function of temperature for theamal processing of titanium electrodes. (Electrolysis conditions: 0.5 M NaCl, 25°C, 30 kA·m^{-2}).

(Figure 10) shows maximal durability in the same temperature range as the lowest potentials (Figure 8).

6. *Activity and Durability vs Catalyst Loading*

The effect of catalyst loading was investigated for 40% RuO_2 coatings treated at 500°C. X-ray analyses have shown that for loadings less than 3 g/m^2 an intermediate layer of TiO_2 appears during thermal treatment while above 3 g/m^2 there is only rutile mixed crystal. Tafel plots for chlorine evolution are displayed in Figure 11 for 4 loadings. Below 5 g/m^2 the Tafel lines are shifted up as the loading decreases and increase in slope at higher current densities. Above 5 g/m^2 the position of the Tafel line is constant (13, 62) but an increase in slope can be seen at about 3 kA/m^2 for the 5 g/m^2 sample although not for the 6.5 g/m^2 one. Electrode potentials at 3 kA/m^2 are plotted against loading in Figure 12 with the optimum lying between 5 and 10 g/m^2.

The loading or thickness of the coating also affects its durability. Figure 13 shows the decrease in lifetime under membrane cell conditions when the loading is lowered to 3 and 1 g/m^2. The TiO_2 layer formed during thermal treatment grows during electrolysis and eventually passivates the electrode especially for thin coatings which do not protect the substrate from anodic

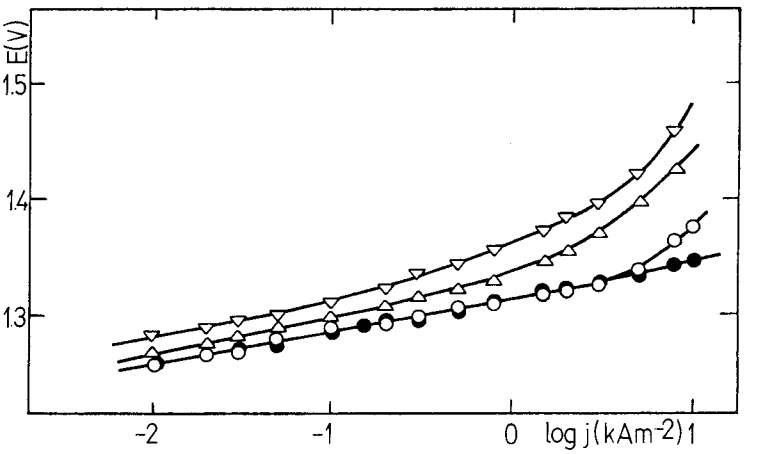

Fig. 11. Polarization characteristics of titanium anodes at optimal coating molar composition (40 mol. % RuO_2) for the chlorine evolution reaction in function of total catalyst amount and thermal processing at 500°C.

●—15, 10 and 6.5 g·m^{-2}; ○-5 g·m^{-2}; △—3g·m^{-2}; ▽—1 g·m^{-2} (Electrolysis conditions: NaCl 300 g·gm^{-3}, pH 2, 80°C).

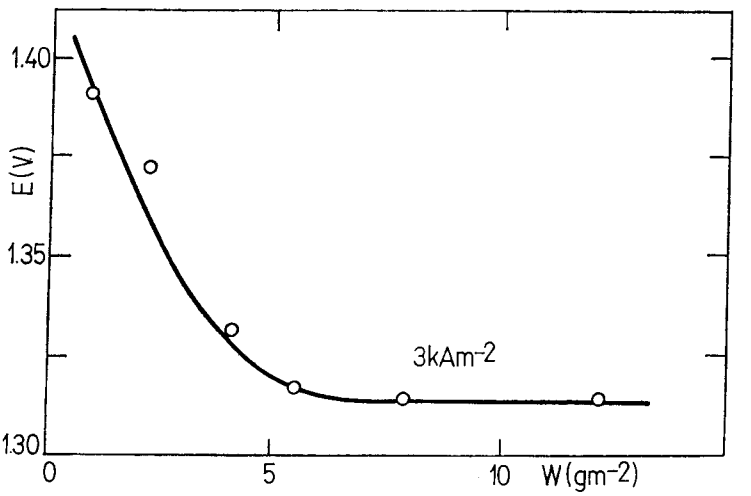

Fig. 12. The effect of total amount of catalyst (40 mol. % RuO_2) on the potential of titanium anodes at constant current density for the chlorine evolution reaction (Electrolysis conditions: NaCl 300 g·dm^{-3}, pH 2, 80°C).

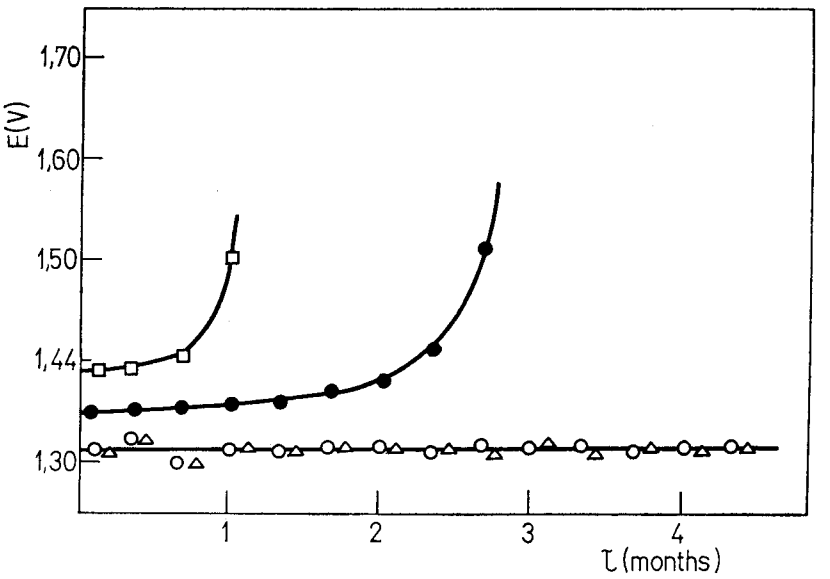

Fig. 13. Titanium anode time—potential function for the chlorine evolution reaction at constant current density and an optimal coating composition (40 mol. % RuO_2) in dependence of the total amount of catalyst. ○–15 g·m^{-2}; △—5 g·m^{-2}; ●—3 g·m^{-2} and □—1 g·m^{-2}. (Electrolysis conditions: NaCl 300 g·dm^{-3}, pH 2, 80°C, 3kA·m-2).

oxygen as well as thick ones. Loadings greater than 10 g/m^2 have been shown to develop cracks during heating as revealed by SEM photographs. For this reason coatings of more than 15 g/m^2 corrode faster and have a shorter lifetime than those with the optimal loading of 10 g/m^2.

Conclusions

Correlation of structural features, processing variables, polarization characteristics and durability of the electrocatalytic coating revealed the conditions (% RuO_2, loading, thermal treatment) necessary to obtain anodes with optimal properties. This work has also elucidated the mechanism by which anode failure occurs and shown that the coating composition and structure determine the catalyst activity and durability.

Acknowledgements

The authors are gratefully indebted to Dr. Norman W. Meyers, ERCO Industries Limited, Islington, Ontario for his personal interest in the present work and his contribution to direct preparation of the present paper by his

English improvement.

References

1) O. de Nora, Chem. Ing. Techn., **42**, 222 (1970).
2) O. de Nora, Chem. Ing. Techn., **43**, 182 (1971).
3) K. R. Koziol, K. H. Sieberer, H.-C. Rathjen, J. B. Zenk and E. F. Wenk, Chem. Ing. Techn., **49**, 288 (1977).
4) D. Bergner, H. Hund and H. Schafer, Chem. Ing. Techn., **47**, 136 (1975).
5) W. A. Gerrard and B. C. H. Steele, J. Appl. Electrochem., **8**, 417 (1978).
6) J. M. Fletcher, W. E. Gardner, B. F. Greenfield, M. J. Holdoway and M. H. Rand, J. Chem. Soc. A, 653 (1968).
7) S. R. Butler and J. L. Gillson, Mater, Res. Bull., **6**, 81 (1971).
8) F. A. Cotton and J. T. Mague, Inorg, Chem., **5**, 317 (1966).
9) J. B. Goodenough, *Magnetism and the Chemical Bond*, Interscience, New York (1963).
10) H. Chiba, J. Electrochem. Soc., Japan, **3**, 3 (1969).
11) A. B. Nikolskij and A. N. Ryabov, Zn. Neorg. Khim., **10**, 3 (1965).
12) J. Horkans and M. W. Shafer, J. Electrochem. Soc., **124**, 1202 (1977).
13) E. A. Kalonovskii, R. U. Bondar and N. N. Meshkova, Elektrokhimiya, **8**, 1468 (1972).
14) C. Iwakura, R. Hirao and H. Tamura, Electrochim. Acta, **22**, 335 (1977).
15) S. Pizzini, G. Buzzanca, C. Mari, L. Rossi and S. Torchio Mater, Res. Bull., **7**, 449 (1972).
16) G. Lodi, C. Bigli and C. de Asmundis, Mater. Chem., **1**, 177 (1976).
17) C. Iwakura, H. Tada and H. Tamura, Electrochim. Acta, **22**, 217 (1977).
18) L. D. Burke, O. J. Murphy, J. F. O'Neill and S. Venkatesan, J.C.S. Faraday, I, **73**, 1659 (1977).
19) J. Augustynski, L. Balsenc and J. Hinden, J. Electrochem. Soc., **125**, 1093 (1978).
20) L. Burke, O. J. Murphy and J. F. O'Neill, J. Electroanal. Chem., **81**, 391 (1977).
21) G. Lodi, E. Sivieri, A. de Battisti and S. Trasatti, J. Appl. Electrochem., **8**, 135 (1978).
22) S. Trasatti and G. Buzzanca, J. Electroanal. Chem., **29**, App. 1 (1971).
23) W. E. O'Grady, C. Iwakura, J. Huang and E. Yeager, *Electrocatalysis*, The Electrochemical Soc., Princeton, N. J., 286 (1974).
24) I. R. Burrows, J. H. Entwiscle and J. A. Harrison, J. Electroanal. Chem., **77**, 21 (1977).
25) D. Galizzioli, F. Tantardini and S. Trasatti, J. Appl. Electrochem., **4**, 57 (1974).
26) D. Galizzidi, F. Tantardini and S. Trasatti, J. Appl. Electrochem., **5**, 203 (1975).
27) T. Arikado, C. Iwakura and H. Tamura, Electrochim. Acta, **22**, 513 (1977).
28) G. Lodi, C. de Asmundis and P. F. Rossi, Mater. Chem., **2**, 103 (1977).
29) F. Hine, M. Yasuda and T. Yoshida, J. Electrochem. Soc., **124**, 500 (1977).
30) L. M. Elina, V. M. Gitneva, V. I. Bystrov and N. M. Shmygul, Elektrokhimiya, **10**, 68 (1974).

31) A. T. Kuhn and C. J. Mortimer, J. Electrochem. Soc., **120**, 231 (1973).
32) A. T. Kuhn and C. J. Mortimer, J. Appl. Electrochem., **2**, 283 (1972).
33) G. Faita and G. Fiori, J. Appl. Electrochem., **2**, 31 (1972).
34) R. U. Bondar, A. A. Borisova and E. A. Kalinovskii, Elektrokhimiya, **10**, 44 (1974).
35) I. E. Veselovskaya, E. K. Spasskaya, V. A. Sokolov, V. I. Tkachenko and L. M. Yakimenko, Elektrokhimiya, **10**, 70 (1974).
36) D. V. Kokoulina, T. V. Ivanova, Yu. I. Krasovitskaya, Z. I. Kudryavtseva and L. I. Khrishtalik, Elektrokhimiya, **13**, 1511 (1977).
37) V. M. Lebedev, Yu. E. Roginskaya, N. L. Klimsenko, V. I. Bystrov and Yu. N. Venevtsev, Zh. Neorg. Khim., **21**, 2511 (1976).
38) Yu. E. Roginskaya, B. Sh. Galamov, V. M. Lebedev, I. D. Belova and Yu. N. Venevtsev, Zh. Neorg. Khim., **22**, 499 (1977).
39) K. Fukuda, C. Iwakura and H. Tamura, Electrochim. Acta, **24**, 367 (1979).
40) Yu. E. Roginskaya, V. I. Bystrov and D. M. Shub, Zh. Neorg. Khim., **22**, 201 (1977).
41) A. Kozowa, J. Inorg. Nucl. Chem., **21**, 315 (1961).
42) L. Burke and O. J. Murphy, J. Electroanal. Chem., **112**, 39 (1980).
43) Yu. B. Makarychev, E. K. Spasskaya, S. D. Khodkevich and L. M. Yakimenko, Elektrokhimiya, **12**, 994 (1976).
44) Ya. M. Fioshin and I. A. Avrutskaya, Usp. Khim., **44**, 2067 (1975).
45) G. Lodi, C. de Asmundis, S. Ardizzone, E. Sivieri and S. Trasatti, Surf. Technol., **14**, 335 (1981).
46) V. E. Kazarinov, L. I. Krishtalik and Yu. V. Pleskov. Trans. SAEST, **12**, 287 (1977).
47) G. Lodi, G. Zucchini, A. de Battisti, E. Sivieri and S. Trasatti, Mater. Chem., **3**, 179 (1978).
48) S. Ardizzone, A. Carugati and S. Trasatti, J. Electroanal. Chem., **126**, 287 (1981).
49) L. D. Burke, M. E. Lyons, E. J. M. O'Sullivan and D. P. Whelan, J. Electroanal. Chem., **122**, 403 (1981).
50) G. Beni, C. E. Rice and J. L. Shay, J. Electrochem. Soc., **127**, 1342 (1980).
51) S. Ardizzone, P. Siviglia and S. Trasatti, J. Electroanal. Chem., **122**, 395 (1981).
52) V. E. Kazarinov and V. N. Andreev, Elektrokhimiya, **13**, 685 (1977).
53) V. E. Kazarinov and V. N. Andreev, Elektrokhimiya, **14**, 577 (1978).
54) L. D. Burke and T. O. O'Meara, J. Electroanal. Chem., **36**, 25 (1972).
55) D. N. Buckley and L. D. Burke, J. Electroanal. Chem., **52**, 433 (1974).
56) L. D. Burke and T. O. O'Meara, J. C. S. Faraday I, **68**, 839 (1972).
57) L. D. Burke and J. F. O'Neill, J. Electroanal. Chem., **101**, 341 (1979).
58) R. G. Erenburg, L. I. Krishtalik and I. P. Yaroshevskaya, Elektrokhimiya, **11**, 1072 (1975).
59) R. G. Erenburg, L. I. Krishtalik and I. P. Yaroshevskaya, Elektrokhimiya, **11**, 1236 (1975).
60) G. Faita and G. Fiori, J. Electrochem. Soc., **120**, 1702 (1973).
61) S. Trasatti, J. Electrochem. Soc., **120**, 1703 (1973).
62) V. I. Bystrov and O. P. Romashin, Elektrokhimiya, **11**, 1226 (1975).
63) M. Inai, C. Iwakura and H. Tamura, Electrochim. Acta, **24**, 993 (1979).

64) N. Ya. Bune, M. M. Pecherskii and V. V. Losev, Elektrokhimiya **11**, 1382 (1975).
65) N. Ya. Bune, G. A. Shilyaeva, V. V. Losev, Elektrokhimiya, **13**, 1540 (1977).
66) C. Iwakura, K. Hirao and H. Tamura, Electrochim. Acta, **22**, 329 (1977).
67) J. Llopis, I. M. Tardesillas and J. M. Alfayata, Electrochim. Acta, **11**, 623 (1965).
68) J. Llopis, J. M. Gamboa and J. M. Alfayata, Electrochim. Acta, **12**, 57 (1967).
69) V. V. Gorodetskii, M. M. Pecherskii, Ya. B. Skuratnik, M. A. Dembrovskii and V. V. Losev, Elektrokhimiya, **9**, 894 (1973).
70) T. Loucka, J. Appl. Electrochem., **7**, 211 (1977).
71) L. M. Elina, V. M. Gitneva and V. I. Bystrov, Elektrokhimiya, **11**, 1279 (1975).
72) V. I. Bystrov, Elektrokhimiya, **11**, 1902 (1975).
73) M. M. Pecherskii, V. V. Gorodetskii, N. Ya. Bune and V. V. Losev, Elektrokhimiya, **18**, 415 (1982).
74) V. V. Gorodetskii, M. M. Pecherskii, V. B. Yake, N. Ya. Bune, V. B. Busse-Mochukas, V. L. Kubasov, V. V. Losev, Elektrokhimiya, **17**, 513 (1981).
75) F. Hine, M. Yasuda, T. Noda, T. Yoshida and J. Okuda, J. Electrochem. Soc., **126**, 1439 (1979).
76) R. G. Erenburg, L. I. Krishtalik and V. I. Bystrov, Elektrokhimiya, **8**, 1740 (1972).
77) R. G. Erenburg, L. I. Krishtalik and I. P. Yaroshevskaya, Elektrokhimiya, **11**, 1068 (1975).
78) M. Pourbaix, *Atlas d'Equilibres Electrochimques*, Gauthiers-Villars et G., Paris (1961).
79) L. D. Burke and O. J. Murphy, J. Electroanal. Chem., **109**, 199 (1980).